

A bright and high-performance genetically encoded Ca²⁺ indicator based on mNeonGreen fluorescent protein

Landon Zarowny, Abhi Aggarwal, Virginia M.S. Rutten, Ilya Kolb, The GENIE Project, Ronak Patel, Hsin-Yi Huang, Yu-Fen Chang, Tiffany Phan, Richard Kanyo, Misha B. Ahrens, W. Ted Allison, Kaspar Podgorski, and Robert E. Campbell

ACS Sens., **Just Accepted Manuscript** • DOI: 10.1021/acssensors.0c00279 • Publication Date (Web): 23 Jun 2020

Downloaded from pubs.acs.org on June 30, 2020

Just Accepted

“Just Accepted” manuscripts have been peer-reviewed and accepted for publication. They are posted online prior to technical editing, formatting for publication and author proofing. The American Chemical Society provides “Just Accepted” as a service to the research community to expedite the dissemination of scientific material as soon as possible after acceptance. “Just Accepted” manuscripts appear in full in PDF format accompanied by an HTML abstract. “Just Accepted” manuscripts have been fully peer reviewed, but should not be considered the official version of record. They are citable by the Digital Object Identifier (DOI®). “Just Accepted” is an optional service offered to authors. Therefore, the “Just Accepted” Web site may not include all articles that will be published in the journal. After a manuscript is technically edited and formatted, it will be removed from the “Just Accepted” Web site and published as an ASAP article. Note that technical editing may introduce minor changes to the manuscript text and/or graphics which could affect content, and all legal disclaimers and ethical guidelines that apply to the journal pertain. ACS cannot be held responsible for errors or consequences arising from the use of information contained in these “Just Accepted” manuscripts.

1
2
3 **A bright and high-performance genetically encoded Ca²⁺ indicator based on**
4 **mNeonGreen fluorescent protein**
5
6
7
8
9

10 Landon Zarowny^{1,∇}, Abhi Aggarwal^{1,2,∇}, Virginia M.S. Rutten^{2,3}, Ilya Kolb², The GENIE
11 Project², Ronak Patel², Hsin-Yi Huang⁴, Yu-Fen Chang⁴, Tiffany Phan¹, Richard Kanyo⁵,
12 Misha B. Ahrens², W. Ted Allison⁵, Kaspar Podgorski², Robert E. Campbell^{1,6,*}
13
14
15
16
17
18

19 ¹Department of Chemistry, University of Alberta, Edmonton, Alberta, Canada
20

21 ²Janelia Research Campus, Howard Hughes Medical Institute, Ashburn, Virginia, United
22 States
23
24

25 ³Gatsby Computational Neuroscience Unit, UCL, London, UK
26
27

28 ⁴LumiSTAR Biotechnology, Inc. National Biotechnology Research Park, Taipei City 115,
29 Taiwan
30
31

32 ⁵Department of Biological Sciences, University of Alberta, Edmonton, Alberta, Canada
33
34

35 ⁶Department of Chemistry, Graduate School of Science, The University of Tokyo, Tokyo,
36 Japan
37
38

39 *Corresponding Author e-mail: robert.e.campbell@ualberta.ca
40
41

42 [∇] These authors contributed equally.
43
44
45
46
47
48
49
50
51
52
53
54
55
56
57
58
59
60

ABSTRACT

Genetically encodable calcium ion (Ca^{2+}) indicators (GECIs) based on green fluorescent proteins (GFP) are powerful tools for imaging of cell signaling and neural activity in model organisms. Following almost two decades of steady improvements in the *Aequorea victoria* GFP (avGFP)-based GCaMP series of GECIs, the performance of the most recent generation (i.e., GCaMP7) may have reached its practical limit due to the inherent properties of GFP. In an effort to sustain the steady progression towards ever-improved GECIs, we undertook the development of a new GECI based on the bright monomeric GFP, mNeonGreen (mNG). The resulting indicator, mNG-GECO1, is 60% brighter than GCaMP6s *in vitro* and provides comparable performance as demonstrated by imaging Ca^{2+} dynamics in cultured cells, primary neurons, and *in vivo* in larval zebrafish. These results suggest that mNG-GECO1 is a promising next-generation GECI that could inherit the mantle of GCaMP and allow the steady improvement of GECIs to continue for generations to come.

KEYWORDS: *Genetically encoded biosensor, fluorescence imaging, mNeonGreen, calcium ion, neural activity imaging, GECI*

1
2
3 Genetically encodable calcium ion (Ca^{2+}) indicators (GECIs) are a class of single
4 fluorescent protein (FP)-based biosensors that are powerful tools for the visualization of
5
6 Ca^{2+} concentration dynamics both *in vitro* and *in vivo*^{1–3}. As they are genetically encoded,
7
8 GECI expression can be genetically targeted to specific cell types or subcellularly
9
10 localized to specific organelles. Furthermore, their negligible cellular toxicity, minimal
11
12 perturbation of endogenous cellular functions, and biological turnover, make them ideal
13
14 for long-term imaging experiments⁴. The Ca^{2+} -dependent fluorescent response of GECIs
15
16 is routinely used as a proxy for neuronal activity due to the transient changes in Ca^{2+}
17
18 concentration that accompany action potentials^{5–8}. GECIs have facilitated the optical
19
20 recording of thousands of neurons simultaneously in the surgically exposed brains of
21
22 mice⁹. Despite their widespread use by the scientific community, there are some
23
24 properties of GECIs that could be further improved. These properties include faster Ca^{2+}
25
26 response kinetics, higher fluorescent molecular brightness, and minimized contribution to
27
28 Ca^{2+} buffering. Some GECIs have shown aggregation in neurons, and some of the most
29
30 highly optimized GECIs have been demonstrated to cause aberrant cortical activity in
31
32 murine models^{10–12}.

33
34
35 An important issue that is common to all GECIs is their intrinsic Ca^{2+} buffering
36
37 capacity. The Ca^{2+} binding domains of GECIs (calmodulin (CaM) or troponin C (TnC)) act
38
39 as Ca^{2+} buffers within the cell and must necessarily compete with endogenous proteins
40
41 for binding to Ca^{2+} (Refs. 13–16). Comprehensive investigations of this phenomenon are
42
43 limited, but a few reports have indicated abnormal morphology and behavior of neurons
44
45 after long term or high expression of GCaMPs¹⁷. Ca^{2+} buffering and competition for CaM
46
47 binding sites have been proposed as possible causes. One solution to the Ca^{2+} buffering
48
49
50
51
52
53
54
55
56
57
58
59
60

1
2
3 phenomenon is to reduce the reporter protein expression, leading to a lower
4 concentration of GECI and reduced buffering capacity. However, reduced expression
5 requires increased intensity of excitation light to achieve an equivalent fluorescent signal,
6 which can lead to increased phototoxicity and photobleaching. Another solution is to
7 reduce the number of Ca^{2+} binding sites like that in the TnC-based GECIs, NTnC¹⁸ and
8 YTnC¹⁹. Unfortunately, these indicators have relatively low fluorescence response
9 ($\Delta F/F_{\min} \sim 1$ for NTnC and ~ 10.6 for YTnC) compared to the recent GCaMP7 variants
10 ($\Delta F/F_{\min} \sim 21$ to 145)²⁰. Another possible solution is to develop GECIs with increased
11 brightness such that they could be expressed at a lower concentration while retaining a
12 similar fluorescent intensity with similar intensity of excitation light.
13
14
15
16
17
18
19
20
21
22
23
24
25

26 Further increasing the brightness of GECIs, while retaining high performance
27 comparable to the most recent generation of indicators, would provide improved tools for
28 optical imaging of neuronal activity and decrease the occurrence of experimental artifacts
29 resulting from Ca^{2+} buffering and indicator overexpression¹⁷. Our efforts to realize this
30 advance were inspired, in part, by the advent of a bright and monomeric engineered
31 version of GFP from *Branchiostoma lanceolatum*, mNeonGreen (mNG)²¹. Due to its high
32 brightness and its excellent performance as a subcellular localization tag²¹, mNG is an
33 exceptionally promising starting point from which to develop a brighter GECI.
34
35
36
37
38
39
40
41
42
43

44 Here we introduce an mNG-based genetically encodable Ca²⁺ indicator for optical
45 imaging (mNG-GECO1) that exceeds the brightness of all variants in the GCaMP series
46 while providing performance that is comparable to the latest generation GCaMP variants.
47 Key design differences between mNG-GECO1 and the GCaMP series include the GFP
48
49
50
51
52
53
54
55
56
57
58
59
60

1
2
3 portion (mNG versus avGFP) and the protein topology (non-circularly permuted mNG
4 versus circularly permuted avGFP).
5
6
7
8
9

10 **EXPERIMENTAL SECTION**

11
12 **General procedures.** Synthetic DNA oligonucleotides and gBlocks were purchased from
13 Integrated DNA Technologies. Plastic consumables, restriction endonucleases, Taq
14 polymerase, Phusion polymerase, T4 DNA ligase, deoxynucleotides, DH10B *E. coli*,
15 pBAD/His B plasmid, pcDNA3.1(+) plasmid, Bacterial Protein Extraction Reagent (B-
16 PER), penicillin-streptomycin, Fetal Bovine Serum (FBS), TurboFect, Lipofectamine
17 2000, and GeneJet gel or plasmid purification kits were purchased from Thermo Fisher
18 Scientific. Endotoxin-free plasmid DNA isolation kits were purchased from Qiagen (cat.
19 12362). Agarose, $\text{MnCl}_2 \cdot 4\text{H}_2\text{O}$, tryptone, D-glucose, ampicillin, L-arabinose, Hank's
20 balanced salt solution (HBSS), DMEM, TrypLE Express, and LB Lennox media were
21 purchased from Fisher Scientific. NbActiv4 and neuron transfection media were
22 purchased from Brain Bits.
23
24
25
26
27
28
29
30
31
32
33
34
35
36

37 3-(N-morpholino)propanesulfonic acid (MOPS), ethylene glycol-bis(2-
38 aminoethylether)-N,N,N',N'-tetraacetic acid (EGTA), and nitrilotriacetic acid (NTA), were
39 purchased from VWR. Nickel NTA immobilized metal affinity chromatography protein
40 purification beads were purchased from G-BioSciences. Ionomycin and tricaine
41 methanesulfonate were purchased from Millipore-Sigma. Ethidium bromide and PCR
42 machines (T100 Thermal Cycler) were purchased from BioRad. Gibson Assembly
43 reagent was purchased from New England Biolabs (NEB). Genemorph II Random
44 Mutagenesis kits and QuikChange mutagenesis kits were purchased from Agilent
45
46
47
48
49
50
51
52
53
54
55
56
57
58
59
60

1
2
3 Technologies. Nunc 96-Well Polypropylene DeepWell Storage Plates (cat. 278743) and
4
5 96-well Nunc MicroWell 96-Well Optical-Bottom Plates (cat. 265301) were purchased
6
7 from Thermo Fisher Scientific. Molecular weight cut off filters were purchased from
8
9 Millipore-Sigma. Sequencing was completed by the Molecular Biology Services Unit at
10
11 the University of Alberta.
12
13
14
15
16

17 **Molecular biology and protein engineering.** Libraries for iterative directed evolution
18
19 were created using Genemorph II Random Mutagenesis kits and NEB's Gibson Assembly
20
21 reagent. Blunt ended linear DNA fragments with random mutations were created using
22
23 the Genemorph II kit according to the manufacturer's recommendations. Genemorph II
24
25 PCR product was ligated using NEB Gibson Assembly reagent into a linearized pBAD
26
27 vector cut with XhoI/HindIII. Site saturation mutagenesis libraries were created using
28
29 single and multi QuikChange mutagenesis kits according the manufacturers
30
31 recommendations.
32
33
34

35 Plasmid libraries were used to transform DH10B *E. coli* which were then plated on
36
37 100 µg ampicillin, 1.5% agar, plates with 0.02% L-arabinose and grown overnight (12-18
38
39 hours) at 37 °C. Colonies were selected on the basis of fluorescence intensity, picked,
40
41 and placed into 96-well DeepWell blocks containing 1.3 mL of LB Lennox media
42
43 supplemented with 100 µg/mL ampicillin and 0.02% L-arabinose. DeepWell blocks were
44
45 shaken overnight at 37 °C. The next day, blocks were centrifuged at 6000 × g for 5
46
47 minutes to pellet cells. Media was discarded and 30 µL of B-PER was added to each well.
48
49 After shaking for 15 minutes, 200 µL of 10 mM EGTA in 30 mM MOPS/100 mM KCl pH
50
51 7.2 (MOPS/KCl buffer) was added to each well of the blocks before mixing briefly and
52
53
54
55
56
57
58
59
60

1
2
3 being centrifuged again for 5 minutes at $6000 \times g$. 90 μL of the resulting lysate was loaded
4
5 in each well of 96-well optical bottom plates. Fluorescence intensity for each well of the
6
7 plate was read with a Tecan Safire² microplate reader to determine the low Ca^{2+} intensity
8
9 for each variant. High Ca^{2+} intensity was acquired by adding 15 μL of 100 mM Ca^{2+} in 30
10
11 mM MOPS pH 7.2 with a 60 second shake before reading. Taking the value of the high
12
13 Ca^{2+} intensity divided by the low Ca^{2+} intensity gives a relative sensitivity value. Promising
14
15 candidates, usually 8-10 variants from each 96-well block, were retested from the lysate
16
17 in 10 mM low (EGTA chelated) and 10 mM high Ca^{2+} solution diluted in MOPS/KCl buffer.
18
19 The plasmids associated with the promising variants were sent for sequencing and used
20
21 as template for the next round of directed evolution. For cultured neuron field stimulation
22
23 experiments, GCaMP6s, jGCaMP7f, jGCaMP7s, jGCaMP7c, and jGCaMP7b plasmids
24
25 (available on Addgene) were subcloned into a syn-*GCaMP*-IRES-mCherry-WPRE-pA
26
27 vector.
28
29
30
31
32

33 Constructs for zebrafish transfection were created by ligating mNG-GECO1 PCR
34
35 product into a Tol2 transposon backbone. Briefly, PCR of mNG-GECO variants were
36
37 ligated into Tol2-HuC-H2B vector (Addgene plasmid #59530) cut with Sall/AgeI using
38
39 Gibson Assembly. The ligated constructs were transformed into NEB Turbo Competent
40
41 *E. coli* cells and grown in 250 μL culture overnight at 30 °C. The next day, the culture was
42
43 pelleted, and the DNA purified using endotoxin-free plasmid DNA purification protocol
44
45 using EndoFree Plasmid Maxi Kit. The DNA was eluted with EF-free H_2O and verified by
46
47 sequencing.
48
49
50
51
52
53
54
55
56
57
58
59
60

1
2
3 **Protein purification and *in vitro* characterization.** To purify mNG, mNG-GECO
4 variants, and GCaMP6s for *in vitro* characterization, pBAD/His B plasmid containing the
5 gene of interest was used to transform electrocompetent DH10B *E. coli*, which were then
6 streaked on 100 µg/mL ampicillin/1.5% agar plates. After overnight incubation at 37 °C,
7
8 a single colony was picked and inoculated to a 2 L flask containing 500 mL of 100 µg/mL
9
10 ampicillin/0.02% L-arabinose liquid media and cultured for 24-30 hours at 37 °C. The
11
12 culture was then centrifuged at 6000 × g for 6 minutes to pellet the cells. Cells were
13
14 resuspended in 30 mL of cold Tris buffered saline (TBS, 150 mM NaCl, 50 mM Tris-HCl)
15
16 pH 8.0 and lysed by sonication (QSonica Q700, amplitude 50, 1 second on, 2 seconds
17
18 off, 3 minutes sonication time). All subsequent purification procedures were performed on
19
20 ice. The resulting lysate was clarified of cell debris by centrifugation for 1 hour at 21,000
21
22 × g, filtered through a Kimwipe™ into a 50 mL conical bottom tube, and incubated for 3
23
24 hours with Ni-NTA resin. Resin containing NTA bound protein was washed with 100 mL
25
26 of 20 mM imidazole TBS wash buffer and eluted with 250 mM imidazole TBS elution
27
28 buffer. Purified protein was buffer exchanged into TBS using a 10,000 Da molecular
29
30 weight cut-off filter (Millipore-Sigma) through 3 successive washes. Absorption spectra
31
32 were recorded on a Beckman-Coulter DU-800 UV-visible spectrophotometer and
33
34 fluorescence spectra recorded on a Tecan Safire² plate reader.
35
36
37
38
39
40
41
42
43

44
45 Quantum yield determination for mNG-GECO variants was performed using mNG
46
47 as a standard²². Briefly, the concentration of protein was adjusted by dilution in MOPS/KCl
48
49 pH 7.2 to reach an absorbance of 0.6 to 1.0. A dilution series with MOPS/KCl and 10 mM
50
51 Ca²⁺ was then prepared with absorbances of 0.01, 0.02, 0.03, 0.04, and 0.05 for mNG,
52
53 mNG-GECO variants, and GCaMP6s. Integration of the fluorescent peaks provides a total
54
55
56
57
58
59
60

1
2
3 fluorescent emission value which was plotted against the absorbance to provide a slope.

4
5 The quantum yields of mNG-GECO variants were determined using the published²² QY
6 value of mNG in a ratiometric manner: ($\Phi_{\text{protein}} = \Phi_{\text{standard}} \times (S_{\text{protein}}/S_{\text{standard}})$).

7
8
9
10 Extinction coefficients were determined using the alkaline denaturation method by
11 measuring the absorption spectrum in MOPS/KCl pH 7.2 and 2 M NaOH. The absorbance
12 value for the denatured GFP peak at 440 nm was divided by the previously determined
13 extinction coefficient of 44,000 M⁻¹cm⁻¹ to give the concentration of protein²². Using Beer's
14 law, the extinction coefficient was then determined by dividing the MOPS/KCl buffered
15 sample absorbance maximum by the calculated protein concentration.

16
17
18
19 Determination of K_d was performed as previously described^{23,24}. Briefly, a
20 reciprocal dilution series was created with either 10 mM EGTA/10 mM CaEGTA ranging
21 in free Ca²⁺ concentration of 0 to 0.039 mM or 10 mM NTA/10 mM Ca²⁺ NTA ranging in
22 free Ca²⁺ concentration from 0 to 1.13 mM²⁴. An equal amount of purified mNG-GECO
23 was diluted 100× into 100 μL of buffer and the intensity plotted against free Ca²⁺ in
24 triplicate. The data were then fit to a 4-parameter variable-slope in GraphPad Prism 7
25 software to determine the K_d .

26
27
28
29
30
31
32
33
34
35
36
37
38
39
40
41
42 **Two-Photon Measurements.** The two-photon measurements were performed in 39 μM
43 free Ca²⁺ (+Ca²⁺) buffer (30 mM MOPS, 10 mM CaEGTA in 100 mM KCl, pH 7.2) or 0 μM
44 free Ca²⁺ (-Ca²⁺) buffer (30 mM MOPS, 10 mM EGTA in 100 mM KCl, pH 7.2). The two-
45 photon excitation spectra were acquired as previously described². Protein solution of 2 –
46 4 μM concentration in +Ca²⁺ or -Ca²⁺ buffer was prepared and measured using an inverted
47 microscope (IX81, Olympus) equipped with a 60×, 1.2 NA water immersion objective
48
49
50
51
52
53
54
55
56
57
58
59
60

1
2
3 (Olympus). Two-photon excitation was obtained using an 80 MHz Ti-Sapphire laser
4
5 (Chameleon Ultra II, Coherent) for spectra from 710 nm to 1080 nm. Fluorescence
6
7 collected by the objective was passed through a short pass filter (720SP, Semrock) and
8
9 a band pass filter (550BP200, Semrock), and detected by a fiber-coupled Avalanche
10
11 Photodiode (APD) (SPCM_AQRH-14, Perkin Elmer). The obtained two-photon excitation
12
13 spectra were normalized for 1 μM concentration and further used to obtain the action
14
15 cross-section spectra (AXS) with fluorescein as a reference²⁵.
16
17
18

19
20 Fluorescence correlation spectroscopy (FCS) was used to obtain the two-photon
21
22 molecular brightness of the protein molecule. The molecular brightness was defined by
23
24 the rate of fluorescence obtained per total number of emitting molecules. 50-200 nM
25
26 protein solutions were prepared in $+\text{Ca}^{2+}$ buffer and excited with 940 nm wavelength at
27
28 various power ranging from 2-30 mW for 200 seconds. The obtained fluorescence was
29
30 collected by an APD and fed to an autocorrelator (Flex03LQ, Correlator.com). The
31
32 obtained autocorrelation curve was fit on a diffusion model through an inbuilt Matlab
33
34 function²⁶ to determine the number of molecules $\langle N \rangle$ present in the focal volume. The
35
36 two-photon molecular brightness (ϵ) at each laser power was calculated as the average
37
38 rate of fluorescence $\langle F \rangle$ per emitting molecule $\langle N \rangle$, defined as $\epsilon = \langle F \rangle / \langle N \rangle$ in kilocounts
39
40 per second per molecule (kcpsm). As a function of laser power, the molecular brightness
41
42 initially increases with increasing laser power, then levels off and decreases due to
43
44 photobleaching or saturation of the protein chromophore in the excitation volume. The
45
46 maximum or peak brightness achieved, $\langle \epsilon_{max} \rangle$, represents a proxy for the photostability
47
48 of a fluorophore.
49
50
51
52
53
54
55
56
57
58
59
60

1
2
3 ***In vitro* kinetics analysis by stopped-flow.** Rapid kinetic measurements of purified
4 mNG-GECO1 and GCaMP6s were made using an Applied Photophysics SX-20 Stopped-
5 flow Reaction Analyzer exciting at 488 nm with 2 nm bandwidth and collecting light at 520
6 nm through a 10 mm path at room temperature. Briefly, 2 μM of mNG-GECO1 and
7 GCaMP6s proteins in 1 mM Ca^{2+} (30 mM MOPS, 100 mM KCl, pH 7.2) were rapidly mixed
8 at 1:1 ratio with 50 mM of EGTA (same buffer as above) at room temperature. k_{off} values
9 were determined by fitting a single exponential dissociation curve to the signal decay
10 using Graphpad Prism, with units of s^{-1} . For k_{on} , both proteins buffered in 30 mM MOPS,
11 100 mM KCl, 50 μM EGTA were rapidly mixed at 1:1 ratio with varying concentrations of
12 Ca^{2+} produced by reciprocal dilutions of 10 mM EGTA and 10 mM CaEGTA. The
13 measured fluorescence change overtime was fitted using a 2-phase association curve to
14 obtain the slow and fast observed rate constants (k_{obs}) for each free Ca^{2+} concentration.
15 All measurements were done in triplicates, and values are reported as mean \pm s.e.m.
16 where noted.
17
18
19
20
21
22
23
24
25
26
27
28
29
30
31
32
33
34
35
36
37

38 **Ca^{2+} imaging in HeLa cells.** We followed previously reported protocols for our Ca^{2+}
39 imaging experiments²⁷ Briefly, HeLa cells cultured in DMEM with 10% fetal bovine serum
40 supplemented with penicillin-G potassium salt (50 units/mL) and streptomycin sulphate
41 (50 $\mu\text{g}/\text{mL}$) were plated on collagen coated 35 mm glass bottom dishes. HeLa cells are
42 transfected at 60% confluency with 1 μg of pcDNA3.1(+) harboring the variant of interest
43 using 2 μL of TurboFect according to the manufacturer's recommendation. After overnight
44 incubation at 37 $^{\circ}\text{C}$ with 5% CO_2 , cells were washed twice with prewarmed Hank's
45 balanced salt solution immediately before imaging. Imaging of transfected HeLa cells was
46
47
48
49
50
51
52
53
54
55
56
57
58
59
60

1
2
3 performed on an inverted Zeiss 200M microscope with Semrock filters (excitation 470/40,
4 emission 525/50) and captured with an OrcaFlash 4.0 – C13440 (Hamamatsu). Images
5 were acquired through a 40× (N.A. 1.3) oil immersion lens using MetaMorph 7.8.0.0
6 software and an MS-2000 automated stage (Applied Scientific Instrumentation).
7
8
9

10
11
12
13
14 **Ca²⁺ imaging in dissociated rat cortical neurons.** The mNG-GECO1 indicator was
15 compared to other GECIs in a field stimulation assay²⁸. Neonatal (P0) rat pups were
16 euthanized, and their cortices were dissected and dissociated using papain
17 (Worthington). Cells were transfected by combining 5×10^5 viable cells with 400 ng
18 plasmid DNA and nucleofection solution electroporation cuvettes (Lonza). Electroporation
19 was performed according to the manufacturer instructions. Cells were then plated at a
20 density of 5×10^5 cells/well in poly-D-lysine (PDL) coated 96-well plates. After 14-18 days
21 *in vitro*, culture medium was exchanged for an imaging buffer solution with a drug cocktail
22 to inhibit synaptic transmission²⁸. The field stimulation assay was performed as previously
23 described^{4,20,28}. Briefly, neurons were field stimulated (1, 2, 3, 5, 10, 20, 40, 160 pulses
24 at 83 Hz, 1 ms, 40V), and concurrently imaged with an electron multiplying charge
25 coupled device (EMCCD) camera (Andor iXon DU897-BV, 198 Hz, 4 × 4 binning, 800 ×
26 800 μm, 1,400 frames). Reference images were taken after stimulation to perform cell
27 segmentation during analysis. Illumination was delivered by blue light (470 nm, Cairn
28 Research Ltd; excitation: 450-490 nm; emission: 500-550 nm; dichroic: 495 nm long-
29 pass). The illumination power density was measured to be 19 mW/mm² at the sample.
30 Stimulation pulses were synchronized with the camera using data acquisition cards
31 (National Instruments), controlled with Wavesurfer software (wavesurfer.janelia.org).
32
33
34
35
36
37
38
39
40
41
42
43
44
45
46
47
48
49
50
51
52
53
54
55
56
57
58
59
60

1
2
3 Imaging was performed at room temperature. Data were analyzed using previously-
4 developed MATLAB (Mathworks) scripts^{20,28}.
5
6
7
8
9

10 **Ca²⁺ imaging in human iPSC-derived cardiomyocytes.** Human iPSC-derived
11 cardiomyocytes (human iPSC Cardiomyocytes - male | ax2505) were purchased from
12 Axol Bioscience. The 96-well glass-bottom plate or MatTek glass bottom dish (Ashland,
13 MA, US) were first coated with fibronectin/gelatin (0.5% / 0.1%) at 37 °C for at least 1
14 hour. The cells were plated and cultured for 3 days in Axol's Cardiomyocyte Maintenance
15 Medium. The cells then were ready for final observation with Tyrode's buffer. For electrical
16 stimulations, iPSC derived cardiomyocytes were plated on MatTek glass bottom dish
17 (Ashland, MA, US) at 100,000 cells/well. Electrical stimulation was done with 10 V, 10 ms
18 duration and 3 seconds interval using myopacer (Ion optix c-pace ep). To image, an
19 inverted microscope (DMi8, Leica) equipped with a 63× objective lens (NA 1.4) and a
20 multiwavelength LED light source (pE-4000, CoolLED) was used. iPSC derived
21 cardiomyocytes were plated out as above, and then loaded with 5 μM Fluo-4-AM (Thermo
22 Fisher Scientific) at room temperature for 10 minutes, free dye was washed off by media
23 replacement with pre-heated culture media, followed by imaging with iXon EMCCD
24 (Andor) camera using 488 nm LED illumination. The GFP filter set (DS/FF02-485/20-25,
25 T495lpxr dichroic mirror, and ET525/50 emission filter) was used for Fluo-4 and mNG-
26 GECO1 observation.
27
28
29
30
31
32
33
34
35
36
37
38
39
40
41
42
43
44
45
46
47
48
49
50

51 **Ca²⁺ imaging in zebrafish larvae.** To demonstrate the sensitivity and brightness of
52 mNG-GECO1 *in vivo*, we performed fluorescence imaging of Ca²⁺ activity in a subset of
53
54
55
56
57
58
59
60

1
2
3 neurons in larval zebrafish. Initially, we used the AB/WIK zebrafish strain for morphology
4 studies (**Supplementary Fig. 4**), which were treated with 1-phenol-2-thiourea (PTU) to
5 inhibit pigmentation, as described previously²⁹. Later, *Casper* strains were available and
6
7 20 ng/ μ L DNA plasmids encoding mNG-GECO1 under the control of nuclear-localized
8 elavl3/HuC promoter (Addgene plasmid #59530) were injected into 2-cell stage embryos
9
10 of *Casper* mutant zebrafish²⁴ with 40 ng/ μ l Tol2 transposase mRNA³⁰ to generate F0
11 transgenic zebrafish. Imaging experiments were performed using 6 day old embryos.
12
13 Embryos showing expression were treated with 1 mg/mL bath-applied α -bungarotoxin
14 (Thermo Fisher Scientific, cat. B1601) dissolved in external solution for 30 seconds to
15 block movement, and subsequently incubated with 80 mM 4-aminopyridine (4AP) for 10
16 minutes. After incubation, the larvae were embedded in 2% low melting temperature
17 agarose to prevent motion. For earlier imaging (**Supplementary Fig. 4**) a Zeiss 700
18 confocal microscope was used with A-Plan 10 \times /0.25 Ph1 M27 objective lens to obtain
19 images of the whole larvae (**Supplementary Fig. 4a**). For enlarged areas
20 (**Supplementary Fig. 4b-e**), a Plan-Apochromat 20 \times /0.8 M27 lens was used. Later
21 imaging was performed using a 488 nm laser (0.45 μ M) and a 525/50 nm emission filter
22 at 3 Hz using Zeiss 880 confocal microscope. The laser power was set to 2.3%, gain 720,
23 and pinhole to 29.3% open. Image acquisition, data registration, segmentation and cell
24 traces were handled using the Suite2p package in Python³¹. All animal procedures were
25 approved by the Institutional Animal Care and Use Committee at the HHMI Janelia
26 Research Campus or by the Animal Care and Use Committee: Biosciences at the
27 University of Alberta.
28
29
30
31
32
33
34
35
36
37
38
39
40
41
42
43
44
45
46
47
48
49
50
51
52
53
54
55
56
57
58
59
60

RESULTS AND DISCUSSION

Rational engineering and iterative directed evolution of mNG-GECO1. We used a combination of rational design, linker sequence optimization, and directed evolution to develop mNG-GECO1 (**Supplementary Fig. 1**). Starting from an unpublished topological variant of REX-GECO1³², we used PCR to produce a fragment containing CaM linked to the RS20 peptide with a short linker (**Fig. 1a**). Insertion of this PCR fragment into the mNG gene between residues 136 and 137 (numbering as in PDB ID 5LTR)³³ resulted in a green fluorescent indicator prototype which we named mNG-GECO0.1 (**Fig. 1**). For the remainder of this manuscript, amino acids will be numbered as in the sequence alignment provided as **Supplementary Fig. 2**. mNG-GECO0.1 had a minimal response to Ca²⁺ ($\Delta F/F_{\min} = 0.3$), but we anticipated that optimization of the sequence around the insertion site would yield a suitable template for directed evolution. Indeed, we found that deletion of Ala146, the residue immediately preceding the insertion of the Ca²⁺ sensing domain, substantially improved the response to Ca²⁺ (mNG-GECO0.2; $\Delta F/F_{\min} \sim 2$).

Starting from mNG-GECO0.2, we began a process of iterative directed evolution which involved screening of libraries created from error-prone PCR or site saturation mutagenesis to identify variants with increased brightness and increased response to Ca²⁺. In our primary library screen, we used a fluorescent colony screening system equipped with excitation and emission filters appropriate for imaging of green fluorescence³⁴. Bright colonies were picked and cultured overnight in liquid media. A secondary screen for Ca²⁺ sensitivity was performed the next day using detergent-extracted bacterial lysate. The fluorescence of the lysate for each variant was measured in Ca²⁺ chelating buffer (30 mM MOPS, 100 mM KCl, 10 mM EGTA, pH 7.2), and

1
2
3 subsequently in Ca²⁺ saturating buffer (30 mM MOPS, 100 mM KCl, 10 mM Ca²⁺, pH 7.2).
4
5 Dividing the Ca²⁺ saturated fluorescence by the Ca²⁺ free fluorescence provided an
6
7 approximate but robust measure of each indicator variant's response to Ca²⁺. For each
8
9 round of screening the plasmids were isolated for the six to ten most promising variants
10
11 and sent for sequencing. The pool of these most promising variants was used as the
12
13 template for the next round of library creation and directed evolution.
14
15

16
17 Following seven rounds of iterative directed evolution, *E. coli* colonies harboring
18
19 mNG-GECO0.7 were brightly fluorescent after overnight incubation. However, the Ca²⁺
20
21 response of mNG-GECO0.7 was remained relatively low ($\Delta F/F_{\min} \sim 5$), compared to
22
23 recent generation GCaMP variants. We anticipated that optimization of the linkers
24
25 connecting mNG to the CaM-RS20 domain (mNG-CaM linker and RS20-mNG linker)
26
27 could lead to the identification of variants with improved responses. To optimize these
28
29 linker regions, we used site saturation mutagenesis to produce libraries of all 20 amino
30
31 acids within the three residues connecting mNG to CaM. Individual libraries of Leu133,
32
33 Thr134, and Ala135 were randomized to all 20 amino acids. If a beneficial mutation was
34
35 found, the process was repeated for the remaining amino acids until these libraries were
36
37 exhausted. By screening of these libraries, we identified two mutations of the linker region
38
39 between mNG barrel and CaM: Ala145Gly and Leu143Ile. This variant, mNG-GECO0.9,
40
41 had a $\Delta F/F_{\min} \sim 12$ as measured *in vitro*.
42
43
44
45

46
47 Following optimization of the mNG-CaM linker, multiple site saturation libraries
48
49 were created, using the same methodology as the mNG-CaM linker, for the RS20-mNG
50
51 linker region (residues Glu323, Trp324, Cys325 and Arg326). Screening of these libraries
52
53 led to the identification of a particularly bright variant with a Cys325Asn mutation. This
54
55
56
57
58
59
60

1
2
3 variant, designated mNG-GECO0.9.1, is brighter than mNG-GECO0.9 but has a
4 decreased response to Ca^{2+} of $\Delta F/F_{\min} = 3.5$. In an effort to improve the performance of
5 mNG-GECO0.9.1, we applied site saturations to positions previously found to be mutated
6 during directed evolution. Screening of these libraries for variants with increased
7 brightness and higher $\Delta F/F_{\min}$ led to the identification of a variant with Asp206Gly,
8 Phe209Leu, Pro263Phe, Lys265Ser, Thr346Ile and the reversion of Gly152Glu. This
9 variant was designated as mNG-GECO1. A notable observation from the directed
10 evolution efforts is the minimal number of mutations in the mNG domain. Only two
11 mutations (Lys128Glu and Thr346Ile) were outside the β -strand in which the Ca^{2+} sensing
12 domain was inserted. In contrast, three mutations were localized to the β -strand
13 surrounding the sensing domain insertion site (Leu143Ile/Ala145Gly/Cys325Asn) and
14 seven mutations (Thr151Ala, Thr180Cys, Asp206Gly, Phe209Leu, Pro263Phe,
15 Lys265Ser, and Ala293Gly) were localized to the CaM domain.
16
17
18
19
20
21
22
23
24
25
26
27
28
29
30
31
32
33
34

35 ***In vitro* characterization of mNG-GECO1.** We characterized mNG-GECO1, in parallel
36 with GCaMP6s, for direct comparison of biophysical properties measured under identical
37 conditions (**Supplementary Table 1**). We found that the excitation (ex) and emission
38 (em) maxima of the Ca^{2+} saturated states to be 497 nm (ex) and 512 nm (em) for
39 GCaMP6s and 496 nm (ex) and 513 nm (em) for mNG-GECO1 (**Fig. 1**). The *in vitro* Ca^{2+}
40 response of mNG-GECO1 ($\Delta F/F_{\min} = 35$) was similar to that of GCaMP6s when tested in
41 parallel ($\Delta F/F_{\min} = 39$). The K_d of mNG-GECO1 (807 nM) is substantially higher than that
42 of GCaMP6s (147 nM). mNG-GECO1 exhibits slightly faster k_{off} kinetics ($k_{\text{off}} = 1.57 \pm$
43
44
45
46
47
48
49
50
51
52
53
54
55
56
57
58
59
60

1
2
3 0.01 s⁻¹) than GCaMP6s ($k_{\text{off}} = 1.06 \pm 0.01 \text{ s}^{-1}$) and similar k_{on} kinetics (**Supplementary**
4
5 **Fig. 3**).

6
7 In the Ca²⁺ bound state, mNG-GECO1 has an extinction coefficient (EC) of
8
9 102,000 M⁻¹cm⁻¹ and quantum yield (QY) of 0.69, giving it an overall brightness (= EC ×
10
11 QY) of 70. This value is similar to the value of 77 previously reported for NTnC¹⁸ and 78%
12
13 of the brightness of mNG itself (measured by us to be 112,000 M⁻¹cm⁻¹ × 0.8 = 90)
14
15 (**Supplementary Fig. 4**). Under two-photon excitation conditions, both mNG-GECO1 and
16
17 GCaMP6s have a maximal two-photon cross section at ~ 970 nm and similar action cross-
18
19 section (AXS) values of 37.22 GM for mNG-GECO1 and 38.81 GM for GCaMP6s.
20
21 However, due to its higher brightness at the single molecule level, the molecular
22
23 brightness of mNG-GECO1 (21.3) is higher than that of GCaMP6s (16.1) at 15 mW
24
25 power. Overall, these data indicate the mNG-GECO1 has excellent one-photon and two-
26
27 photon excitation properties *in vitro*.
28
29
30
31
32
33
34

35 ***In vitro* characterization in cultured cells and dissociated neurons.** To compare the
36
37 performance of mNG-GECO1 and GCaMP6s in cultured cells, we transfected HeLa cells
38
39 with mNG-GECO1 in a pcDNA vector (CMV promoter) in parallel with pGP-CMV-
40
41 GCaMP6s. Using a previously reported protocol²⁷, Ca²⁺ oscillations were induced by
42
43 treatment with histamine and fluorescence images were acquired every 10 seconds for
44
45 20 minutes. From the intensity versus time data for each cell, $\Delta F/F_0$ for all oscillations of
46
47 $\Delta F/F_0 > 0.5$ were extracted using a Matlab script. Using these extracted $\Delta F/F_0$ values,
48
49 average $\Delta F/F_0$ for all oscillations and maximum $\Delta F/F_0$ was computed. The average
50
51 maximum $\Delta F/F_0$ was calculated by averaging the maximum $\Delta F/F_0$ from each responding
52
53
54
55
56
57
58
59
60

1
2
3 cell. In parallel experiments, mNG-GECO1 had an average $\Delta F/F_0 = 4.50 \pm 2.96$ compared
4
5 to GCaMP6s's $\Delta F/F_0 = 3.48 \pm 2.40$ (**Fig. 1h**). The maximum $\Delta F/F_0$ was 16.8 ± 10.5 for
6
7 mNG-GECO1 and 12.8 ± 6.11 for GCaMP6s. At the end of the 20 minute imaging
8
9 experiment, the cells were treated with ionomycin/ Ca^{2+} to saturate the indicators and
10
11 induce a fluorescent maximum and then with Ca^{2+} chelator EGTA/ionomycin to deplete
12
13 Ca^{2+} and produce a fluorescent minimum. For these treatments, $\Delta F/F_{\text{min}} = 48.8 \pm 15.1$ for
14
15 mNG-GECO1 and $\Delta F/F_{\text{min}} = 16.7 \pm 5.2$ for GCaMP6s. These results were obtained from
16
17 a data set of 137 responding cells with 1624 individual oscillations for mNG-GECO1 and
18
19 99 responding cells with 687 individual oscillations for GCaMP6s (**Supplementary Table**
20
21
22
23
24
25 **2**).

26
27 We next characterized the performance of mNG-GECO1 in dissociated rat cortical
28
29 neurons alongside GCaMP series indicators GCaMP6s, jGCaMP7s, jGCaMP7b,
30
31 jGCaMP7c, and jGCaMP7f (**Fig. 2**). Field stimulated neurons expressing mNG-GECO1
32
33 had a single action potential (AP) $\Delta F/F_0 = 0.19 \pm 0.04$, slightly lower than that of GCaMP6s
34
35 ($\Delta F/F_0 = 0.27 \pm 0.09$, **Fig. 2a**). For 10 APs, performance of mNG-GECO1 was
36
37 approximately 2-fold lower than GCaMP6s, with $\Delta F/F_0$ of 1.5 ± 0.19 and 3.1 ± 0.26 for
38
39 mNG-GECO1 and GCaMP6s, respectively (**Fig. 2b**). At 160 APs, mNG-GECO1 has a
40
41 $\Delta F/F_0$ of 6.5 ± 0.8 , slightly lower than GCaMP6s's $\Delta F/F_0$ of 9.0 ± 0.47 (**Fig. 2c**). The
42
43 baseline brightness of mNG-GECO1 ($1,374 \pm 31$ AU) was comparable to the baseline
44
45 brightness of GCaMP6s ($1,302 \pm 6$ AU) and jGCaMP7s ($1,397 \pm 11$ AU) (**Fig. 2e**). The
46
47 signal-to-noise ratio (SNR) of mNG-GECO1 and GCaMP6s are comparable for one and
48
49 three AP's (**Fig. 2f**). For three AP stimulation, mNG-GECO1 exhibited a half rise time of
50
51
52
53
54
55
56
57
58
59
60 49 ± 1 ms and half decay time of 582 ± 12 ms. Under the same conditions, GCaMP6s

1
2
3 exhibited a half rise time of 65 ± 2 ms and a half decay time of $1,000 \pm 36$ ms. Field
4 stimulated neuron data is summarized in **Supplementary Table 3**. The overall data in
5 cultured neurons suggest that the mNG-GECO1 sensor is comparable in signal, kinetics,
6 and baseline brightness to the GCaMP6s sensor.
7
8
9
10
11
12
13

14 ***In vivo* evaluation of mNG-GECO1.** To evaluate mNG-GECO1 for *in vivo* expression in
15 zebrafish neurons, we used a Tol2 transposase transgenesis system to deliver mNG-
16 GECO1 or GCaMP6s under a pan-neuronal Elavl3 promoter into zebrafish embryos³⁰.
17 We tracked expression of mNG-GECO1 over several days to evaluate the viability of
18 transgenic fish (**Supplementary Fig. 5**). We found no obvious morphological anomalies
19 during the larval development stage of zebrafish expressing mNG-GECO1 or GCaMP6s.
20 To evaluate the relative performance of mNG-GECO1 and GCaMP6s for imaging of
21 neuronal activity in zebrafish larvae, we used the same transgenesis protocol to produce
22 *Casper* zebrafish lines expressing each indicator (**Fig. 3**). Prior to imaging, five to six days
23 post fertilization *Casper* fish expressing the sensors were immobilized with bungarotoxin
24 (1 mg/mL) for 30 seconds followed by a 10 minute incubation in the convulsant 80 mM 4-
25 aminopyridine (4-AP). The fish were then placed in low melting agar and immersed in a
26 solution of 4-AP (80 mM). Imaging consisted of 5 minute intervals of the hindbrain or
27 midbrain at a recording rate of 3 Hz. For each indicator, five fish were imaged under six
28 different field of views resulting in 834 and 1280 individual cells for mNG-GECO1 and
29 GCaMP6s, respectively (**Supplementary Fig. 6**). The resulting data was evaluated using
30 the Suite2p package (github.com/MouseLand/suite2p)³¹. We found that mNG-GECO1
31 had a maximum $\Delta F/F_0$ for each cell of 3.09 ± 0.08 compared to 4.56 ± 0.11 for GCaMP6s
32
33
34
35
36
37
38
39
40
41
42
43
44
45
46
47
48
49
50
51
52
53
54
55
56
57
58
59
60

1
2
3 **(Fig. 3c)**. The baseline fluorescence of GCaMP6s was higher compared to mNG-GECO1
4 (1.41 ± 0.05 vs 0.95 ± 0.03 AU, respectively) **(Fig. 3d)**. However, the signal-to-noise ratio
5 (SNR), which was computed by dividing the $\Delta F/F_0$ by the raw standard deviation of each
6 cell in 6 field of views, was higher for mNG-GECO1 (SNR = 6.63 ± 0.07) than GCaMP6s
7 (SNR = 5.25 ± 0.04) **(Fig. 3e)**. We also found that mNG-GECO1 had a shorter decay time
8 (faster k_{off} kinetics) compared to GCaMP6s (1.98 ± 0.12 s versus 3.00 ± 0.12 s,
9 respectively) **(Fig. 3f)**. The overall data in zebrafish neurons suggest that mNG-GECO1
10 is comparable in signal-to-noise ratio, kinetics, and baseline brightness to the GCaMP6s
11 sensor **(Supplementary Table 4)**.
12
13
14
15
16
17
18
19
20
21
22
23
24
25

26 **Ca²⁺ imaging in human iPSC-derived cardiomyocytes.** Chemical Ca²⁺ dyes such as
27 Fluo-4 acetoxymethyl (AM), Rhod-2 AM and Fura-2 AM are often used to phenotype Ca²⁺
28 transients in induced pluripotent stem cell-derived cardiomyocytes (iSPC-CM). However,
29 these dyes can be toxic^{35,36} and may potentially suppress the activity of Na⁺ and K⁺-
30 dependent adenosine triphosphatase³⁷. As such, we tested whether mNG-GECO1 could
31 serve as a robust tool for observing cells signaling and drug response while preventing
32 cellular toxicity in iPSC-CMs **(Supplementary Fig. 7)**. We found that when iPSC-CMs
33 expressing mNG-GECO1 or Fluo-4 AM were treated with 20 mM caffeine, mNG-GECO1
34 had a 2.8-fold higher $\Delta F/F$ response than Fluo-4 ($\Delta F/F$ = 11.77 ± 2.82 and 4.18 ± 1.27,
35 respectively) **(Supplementary Fig. 7a, b)**. However, when cells were subjected to 0.33
36 Hz electrical stimulation for 30 minutes, mNG-GECO1 had a slightly lower peak $\Delta F/F$
37 (2.26 ± 0.81) than Fluo-4 AM (3.31 ± 1.42) **(Supplementary Fig. 7c, d)**. We suspect that
38 this discrepancy is due to mNG-GECO1's lower affinity for Ca²⁺. When we stimulated the
39
40
41
42
43
44
45
46
47
48
49
50
51
52
53
54
55
56
57
58
59
60

1
2
3 cells in the presence of 20 mM caffeine, the max $\Delta F/F$ of mNG-GECO1 ($\Delta F/F = 14.20 \pm$
4 4.67) was higher than the max $\Delta F/F$ of Fluo-4 AM ($\Delta F/F = 6.73 \pm 1.19$) (**Supplementary**
5 **Fig. 7e, f**). Based on this data, we propose that mNG-GECO1 may serve as a useful tool
6 for phenotypic screening and functional tests in iPSC-CMs.
7
8
9
10
11
12
13

14 **SUMMARY**

15
16 mNG-GECO1 is a new, first-generation, genetically encodable Ca^{2+} indicator that
17 provides performance comparable to 6th and 7th generation GCaMP indicators. We have
18 demonstrated that the *in vitro* performance of mNG-GECO1 in cultured HeLa cells is on
19 par or better than GCaMP6s. However, *in vitro* cultured neuron benchmarking as well as
20 *in vivo* imaging in transgenic zebrafish larvae have indicated that further engineering and
21 directed evolution efforts will be required to produce an mNG-GECO1 variant that
22 provides substantial advantages relative to the jGCaMP7 series.
23
24
25
26
27
28
29
30
31
32

33 While this work was under review, Subach *et al.*, reported NCaMP7, a high
34 performance mNG-based GECI with a very similar design to mNG-GECO1 (Ref. 38). Both
35 mNG-GECO1 and NCaMP7 have performance that is comparable to GCaMP6s for *in*
36 *vivo* imaging of neuronal activity, and it remains to be seen how these two indicators
37 compare side-by-side. Based on *in vitro* characterization, mNG-GECO1 is the brighter of
38 the two mNG-based GECIs ($\text{EC} \times \text{QY} = 70$ for mNG-GECO1 and 57 for NCaMP7) while
39 NCaMP7 has the larger fluorescence response ($\Delta F/F_0 = 35$ for mNG-GECO1 and 89 for
40 NCaMP7) and higher Ca^{2+} affinity ($K_d = 807$ nM for mNG-GECO1 and 96 nM for
41 NCaMP7). Together these two indicators clearly demonstrate that mNG is a versatile and
42 promising scaffold for the development of next generation GECIs. Combining the
43
44
45
46
47
48
49
50
51
52
53
54
55
56
57
58
59
60

1
2
3 mutations present is both GECIs, using the NCaMP7 crystal structure as a guide, is a
4 promising approach to developing a substantially improved next generation GECI that
5 could potentially surpass GCaMP7 in terms of overall performance.
6
7
8
9

10 In summary, we have developed a first generation GECI from the mNG scaffold
11 that retains the high fluorescent brightness *in vitro* with performance comparable to the
12 state-of-the-art GECI, GCaMP6s. We expect mNG-GECO1 to be just as amenable to
13 further optimization as the first generation GCaMP, and so mNG-GECO1 is likely to serve
14 as the parent of a new and improved lineage of high performance GECIs.
15
16
17
18
19
20
21
22
23

24 **ASSOCIATED CONTENT**

25
26 Supporting Information Available: The following files are available free of charge.

27
28 File name: mNG-GECO1_Supporting_Information.pdf

29
30 *In vitro* characterization of mNG-GECO1 and GCaMP6s (Supplementary Table 1),
31
32 Characterization of Ca²⁺-dependent fluorescence of mNG-GECO1 and GCaMP6s in
33 HeLa cells (Supplementary Table 2), mNG-GECO1 comparison with GCaMP series
34 sensors in dissociated rat hippocampal neurons (Supplementary Table 3), mNG-GECO1
35 comparison with GCaMP6s in larval zebrafish 6 dpf (Supplementary Table 4), Overview
36 of mNG-GECO1 development (Supplementary Fig. 1), Sequence alignment of mNG-
37 GECO variants (Supplementary Fig. 2), k_{on} traces of mNG-GECO1 and GCaMP6s
38 (Supplementary Fig. 3), *In vitro* brightness comparison of mNG-GECO1 to GCaMP series
39 (Supplementary Fig. 4), mNG-GECO1 expression profile in zebrafish larvae
40 (Supplementary Fig. 5), mNG-GECO1 and GCaMP6s field of views (FOV) in zebrafish
41
42
43
44
45
46
47
48
49
50
51
52
53
54
55
56
57
58
59
60

1
2
3 larvae used for quantification (Supplementary Fig. 6), Comparison of Fluo-4 Ca²⁺ dye and
4
5 mNG-GECO1 in human iPSC-derived cardiomyocytes (Supplementary Fig. 7).
6
7
8
9

10 **AUTHOR INFORMATION**

11 **Corresponding Author**

12
13 *E-mail: robert.e.campbell@ualberta.ca
14
15
16

17 **ORCID**

18
19 Robert E. Campbell: 0000-0003-0604-092X
20
21

22 **Author contributions**

23
24 LZ, AA, and TP performed the directed evolution experiments and *in vitro*
25
26 characterization. RP performed the *in vitro* two-photon characterization, IK and TGP
27
28 conducted and analyzed the cultured neuron experiments. RK conducted the initial
29
30 expression experiments of mNG-GECO1 and its variants in zebrafish under the
31
32 supervision of WTA. VR completed the zebrafish characterization under the supervision
33
34 of MA. HYH and YFC did the experiments in human iPSC-derived cardiomyocytes. LZ,
35
36 AA, KP, and REC wrote and edited the manuscript. LZ and AA contributed equally to this
37
38 work. All authors were allowed to review and edit the manuscript before publication.
39
40
41

42 **Notes**

43
44 The University of Alberta and Allele Biotechnology intend to file a patent application
45
46 describing mNG-GECO1.
47
48
49
50

51 **ACKNOWLEDGEMENTS**

52
53
54
55
56
57
58
59
60

1
2
3 We thank the University of Alberta Molecular Biology Services Unit (University of Alberta)
4 and Molecular Bio (Janelia) for technical support. We thank Christopher Cairo (University
5 of Alberta), Andy Holt (Alberta) and Loren Looger (Janelia) for providing access to the
6 instrumentation, Eric Schreiter (Janelia) for providing access to resources and for useful
7 feedback regarding the manuscript. We thank Deepika Walpia (Janelia) and the JRC
8 Histology group for preparing cultured neurons. We thank John Macklin (Janelia) for
9 overseeing two-photon measurements. We thank Nathan Shaner and coworkers for the
10 development of mNeonGreen fluorescent protein. REC acknowledges the Japan Society
11 for the Promotion of Science (JSPS), Natural Sciences and Engineering Research
12 Council of Canada (NSERC), and Canadian Institutes of Health Research (CIHR), for
13 funding support. The mNeonGreen gene was a kind gift from Jiwu Wang at Allele
14 Biotechnology.

15
16
17
18
19
20
21
22
23
24
25
26
27
28
29
30
31 The GENIE (Genetically Encoded Neuronal Indicators and Effectors) Project
32 (www.janelia.org/project-team/genie) is a team project at the Janelia Research Campus
33 of HHMI set up to optimize the performance of fluorescent indicators for neuroscience
34 applications. For this work, the GENIE project tested the performance of mNG-GECO1
35 relative to GCaMP6 and GCaMP7 in neuron cultures with field stimulation and
36 epifluorescence microscopy.
37
38
39
40
41
42
43
44
45
46

47 REFERENCES

- 48
49 1. Mank, M.; Griesbeck, O., Genetically encoded calcium indicators. *Chem. Rev.*
50 **2008**, *108*, 1550-1564.
51
52
53
54
55
56
57
58
59
60

- 1
2
3 2. Akerboom, J.; Chen, T.-W.; Wardill, T. J.; Tian, L.; Marvin, J. S.; Mutlu, S.;
4
5 Calderón, N. C.; Esposti, F.; Borghuis, B. G.; Sun, X. R., *et al.*, Optimization of a GCaMP
6
7 Calcium Indicator for Neural Activity Imaging. *J. Neurosci.* **2012**, *32*, 13819-13840.
8
9
- 10 3. Knöpfel, T., Genetically encoded optical indicators for the analysis of neuronal
11
12 circuits. *Nat. Rev. Neurosci.* **2012**, *13*, 687-700.
13
- 14 4. Chen, T. W.; Wardill, T. J.; Sun, Y.; Pulver, S. R.; Renninger, S. L.; Baohan, A.;
15
16 Schreiter, E. R.; Kerr, R. A.; Orger, M. B.; Jayaraman, V., *et al.*, Ultrasensitive fluorescent
17
18 proteins for imaging neuronal activity. *Nature* **2013**, *499*, 295-300.
19
- 20 5. Pologruto, T. A.; Yasuda, R.; Svoboda, K., Monitoring neural activity and [Ca²⁺]
21
22 with genetically encoded Ca²⁺ indicators. *J. Neurosci.* **2004**, *24*, 9572-9579.
23
- 24 6. Tian, L.; Akerboom, J.; Schreiter, E. R.; Looger, L. L., Neural activity imaging with
25
26 genetically encoded calcium indicators. *Prog. Brain. Res.* **2012**, *196*, 79-94.
27
- 28 7. Deo, C.; Lavis, L. D., Synthetic and genetically encoded fluorescent neural activity
29
30 indicators. *Curr. Opin. Neurobiol.* **2018**, *50*, 101-108.
31
32
- 33 8. Broussard, G. J.; Liang, R.; Tian, L., Monitoring activity in neural circuits with
34
35 genetically encoded indicators. *Front. Mol. Neurosci.* **2014**, *7*, 97, DOI:
36
37 10.3389/fnmol.2014.00097.
38
39
- 40 9. Kim, T. H.; Zhang, Y.; Lecoq, J.; Jung, J. C.; Li, J.; Zeng, H.; Niell, C. M.; Schnitzer,
41
42 M. J., Long-Term Optical Access to an Estimated One Million Neurons in the Live Mouse
43
44 Cortex. *Cell Rep.* **2016**, *17*, 3385-3394.
45
46
47
- 48 10. Podor, B.; Hu, Y. L.; Ohkura, M.; Nakai, J.; Croll, R.; Fine, A., Comparison of
49
50 genetically encoded calcium indicators for monitoring action potentials in mammalian
51
52
53
54
55
56
57
58

1
2
3 brain by two-photon excitation fluorescence microscopy. *Neurophotonics* **2015**, *2*,
4 021014, DOI: 10.1117/1.NPh.2.2.021014.
5

6
7
8 11. Bootman, M. D.; Allman, S.; Rietdorf, K.; Bultynck, G., Deleterious effects of
9 calcium indicators within cells; an inconvenient truth. *Cell Calcium* **2018**, *73*, 82-87.
10

11
12 12. Steinmetz, N. A.; Buetfering, C.; Lecoq, J.; Lee, C. R.; Peters, A. J.; Jacobs, E. A.
13 K.; Coen, P.; Ollerenshaw, D. R.; Valley, M. T.; de Vries, S. E. J., *et al.*, Aberrant Cortical
14 Activity in Multiple GCaMP6-Expressing Transgenic Mouse Lines. *eNeuro* **2017**, *4*,
15 ENEURO.0207-17.2017, DOI: 10.1523/ENEURO.0207-17.2017.
16
17

18
19 13. Helmchen, F.; Imoto, K.; Sakmann, B., Ca²⁺ buffering and action potential-evoked
20 Ca²⁺ signaling in dendrites of pyramidal neurons. *Biophys. J.* **1996**, *70*, 1069-1081.
21
22

23
24 14. Ashworth, R.; Zimprich, F.; Bolsover, S. R., Buffering intracellular calcium disrupts
25 motoneuron development in intact zebrafish embryos. *Brain Res. Dev. Brain Res.* **2001**,
26 *129*, 169-179.
27
28

29
30 15. Briston, S. J.; Dibb, K. M.; Solaro, R. J.; Eisner, D. A.; Trafford, A. W., Balanced
31 changes in Ca buffering by SERCA and troponin contribute to Ca handling during β -
32 adrenergic stimulation in cardiac myocytes. *Cardiovasc. Res.* **2014**, *104*, 347-354.
33
34

35
36 16. Timofeeva, Y.; Volynski, K. E., Calmodulin as a major calcium buffer shaping
37 vesicular release and short-term synaptic plasticity: facilitation through buffer dislocation.
38 *Front. Cell. Neurosci.* **2015**, *9*, 239-239.
39
40

41
42 17. Yang, Y.; Liu, N.; He, Y.; Liu, Y.; Ge, L.; Zou, L.; Song, S.; Xiong, W.; Liu, X.,
43 Improved calcium sensor GCaMP-X overcomes the calcium channel perturbations
44 induced by the calmodulin in GCaMP. *Nat. Commun.* **2018**, *9*, 1504, DOI:
45 10.1038/s41467-018-03719-6.
46
47
48
49
50
51
52
53
54
55
56
57
58
59
60

- 1
2
3 18. Barykina, N. V.; Subach, O. M.; Doronin, D. A.; Sotskov, V. P.; Roshchina, M. A.;
4 Kunitsyna, T. A.; Malyshev, A. Y.; Smirnov, I. V.; Azieva, A. M.; Sokolov, I. S., *et al.*, A
5 new design for a green calcium indicator with a smaller size and a reduced number of
6 calcium-binding sites. *Sci. Rep.* **2016**, *6*, 34447, DOI: 10.1038/srep34447.
7
8
9
10
11
12 19. Barykina, N. V.; Doronin, D. A.; Subach, O. M.; Sotskov, V. P.; Plusnin, V. V.;
13 Ivleva, O. A.; Gruzdeva, A. M.; Kunitsyna, T. A.; Ivashkina, O. I.; Lazutkin, A. A., *et al.*,
14 NTnC-like genetically encoded calcium indicator with a positive and enhanced response
15 and fast kinetics. *Sci. Rep.* **2018**, *8*, 15233. DOI: 10.1038/s41598-018-33613-6.
16
17
18
19
20
21 20. Dana, H.; Sun, Y.; Mohar, B.; Hulse, B. K.; Kerlin, A. M.; Hasseman, J. P.;
22 Tsegaye, G.; Tsang, A.; Wong, A.; Patel, R., *et al.*, High-performance calcium sensors
23 for imaging activity in neuronal populations and microcompartments. *Nat. Methods* **2019**,
24 *16*, 649-657.
25
26
27
28
29
30
31 21. Shaner, N. C.; Lambert, G. G.; Chammas, A.; Ni, Y.; Cranfill, P. J.; Baird, M. A.;
32 Sell, B. R.; Allen, J. R.; Day, R. N.; Israelsson, M., *et al.*, A bright monomeric green
33 fluorescent protein derived from *Branchiostoma lanceolatum*. *Nat. Methods* **2013**, *10*,
34 407-409.
35
36
37
38
39
40 22. Cranfill, P. J.; Sell, B. R.; Baird, M. A.; Allen, J. R.; Lavagnino, Z.; de Gruiter, H.
41 M.; Kremers, G. J.; Davidson, M. W.; Ustione, A.; Piston, D. W., Quantitative assessment
42 of fluorescent proteins. *Nat. Methods* **2016**, *13*, 557-562.
43
44
45
46
47 23. Tsien, R.; Pozzan, T., Measurement of cytosolic free Ca²⁺ with quin2. In *Methods*
48 *Enzymol.*, Academic Press: **1989**; Vol. 172, pp 230-262.
49
50
51 24. Dweck, D.; Reyes-Alfonso, A.; Potter, J. D., Expanding the range of free calcium
52 regulation in biological solutions. *Anal. Biochem.* **2005**, *347*, 303-315.
53
54
55
56
57
58
59
60

- 1
2
3 25. Xu, C.; Webb, W. W., Measurement of two-photon excitation cross sections of
4 molecular fluorophores with data from 690 to 1050 nm. *J. Opt. Soc. Am. B* **1996**, *13*, 481-
5 491.
6
7
8
9
10 26. Mütze, J.; Iyer, V.; Macklin, John J.; Colonell, J.; Karsh, B.; Petrášek, Z.; Schwille,
11 P.; Looger, Loren L.; Lavis, Luke D.; Harris, Timothy D., Excitation Spectra and
12 Brightness Optimization of Two-Photon Excited Probes. *Biophys. J.* **2012**, *102*, 934-944.
13
14
15
16
17 27. Palmer, A. E.; Tsien, R. Y., Measuring calcium signaling using genetically
18 targetable fluorescent indicators. *Nat. Protoc.* **2006**, *1*, 1057-1065.
19
20
21 28. Wardill, T. J.; Chen, T.-W.; Schreiter, E. R.; Hasseman, J. P.; Tsegaye, G.; Fosque,
22 B. F.; Behnam, R.; Shields, B. C.; Ramirez, M.; Kimmel, B. E., *et al.*, A Neuron-Based
23 Screening Platform for Optimizing Genetically-Encoded Calcium Indicators. *PLoS One*
24 **2013**, *8*, e77728, DOI: 10.1371/journal.pone.0077728.
25
26
27
28
29
30 29. Thorn, R. J.; Clift, D. E.; Ojo, O.; Colwill, R. M.; Creton, R., The loss and recovery
31 of vertebrate vision examined in microplates. *PLoS One* **2017**, *12*, e0183414,
32 DOI: 10.1371/journal.pone.0183414.
33
34
35
36
37 30. Kawakami, K.; Takeda, H.; Kawakami, N.; Kobayashi, M.; Matsuda, N.; Mishina,
38 M., A Transposon-Mediated Gene Trap Approach Identifies Developmentally Regulated
39 Genes in Zebrafish. *Dev. Cell* **2004**, *7*, 133-144.
40
41
42
43
44 31. Pachitariu, M.; Stringer, C.; Dipoppa, M.; Schröder, S.; Rossi, L. F.; Dagleish, H.;
45 Carandini, M.; Harris, K. D., Suite2p: beyond 10,000 neurons with standard two-photon
46 microscopy. *bioRxiv* 2017, 061507, DOI: 10.1101/061507.
47
48
49
50
51 32. Wu, J.; Abdelfattah, A. S.; Miraucourt, L. S.; Kutsarova, E.; Ruangkittisakul, A.;
52 Zhou, H.; Ballanyi, K.; Wicks, G.; Drobizhev, M.; Rebane, A., *et al.*, A long Stokes shift
53
54
55
56
57
58
59
60

1
2
3 red fluorescent Ca²⁺ indicator protein for two-photon and ratiometric imaging. *Nat.*
4
5 *Commun.* **2014**, *5*, 5262, DOI: 10.1038/ncomms6262.

6
7
8 33. Clavel, D.; Gotthard, G.; von Stetten, D.; De Sanctis, D.; Pasquier, H.; Lambert, G.
9
10 G.; Shaner, N. C.; Royant, A., Structural analysis of the bright monomeric yellow-green
11
12 fluorescent protein mNeonGreen obtained by directed evolution. *Acta Crystallogr. D*
13
14 *Struct. Biol.* **2016**, *72*, 1298-1307.

15
16
17 34. Ai, H.-w.; Baird, M. A.; Shen, Y.; Davidson, M. W.; Campbell, R. E., Engineering
18
19 and characterizing monomeric fluorescent proteins for live-cell imaging applications. *Nat.*
20
21 *Protoc.* **2014**, *9*, 910-928.

22
23
24 35. Shinnawi, R.; Huber, I.; Maizels, L.; Shaheen, N.; Gepstein, A.; Arbel, G.; Tijssen,
25
26 Anke J.; Gepstein, L., Monitoring Human-Induced Pluripotent Stem Cell-Derived
27
28 Cardiomyocytes with Genetically Encoded Calcium and Voltage Fluorescent Reporters.
29
30 *Stem Cell Reports* **2015**, *5*, 582-596.

31
32
33 36. Chang, Y.-F.; Broyles, C. N.; Brook, F. A.; Davies, M. J.; Turtle, C. W.; Nagai, T.;
34
35 Daniels, M. J., Non-invasive phenotyping and drug testing in single cardiomyocytes or
36
37 beta-cells by calcium imaging and optogenetics. *PLoS One* **2017**, *12*, e0174181,
38
39 DOI: 10.1371/journal.pone.0174181.

40
41
42 37. Smith, N. A.; Kress, B. T.; Lu, Y.; Chandler-Militello, D.; Benraiss, A.; Nedergaard,
43
44 M., Fluorescent Ca²⁺ indicators directly inhibit the Na,K-ATPase and disrupt cellular
45
46 functions. *Sci. Signal.* **2018**, *11*, eaal2039, DOI: 10.1126/scisignal.aal2039.

47
48
49 38. Subach, O. M.; Sotnikov, V. P.; Plusnin, V. V.; Gruzdeva, A. M.; Barykina, N. V.;
50
51 Ivashkina, O. I.; Anokhin, K. V.; Nikolaeva, A. Y.; Korzhenevskiy, D. A.; Vlaskina, A. V.,
52
53 *et al.*, Novel Genetically Encoded Bright Positive Calcium Indicator NCaMP7 Based on
54
55

1
2
3 the mNeonGreen Fluorescent Protein. *Int. J. Mol. Med. Sci.* **2020**, *21*, 1644, DOI:
4
5 10.3390/ijms21051644.
6
7
8
9
10
11
12
13
14
15
16
17
18
19
20
21
22
23
24
25
26
27
28
29
30
31
32
33
34
35
36
37
38
39
40
41
42
43
44
45
46
47
48
49
50
51
52
53
54
55
56
57
58
59
60

FIGURES

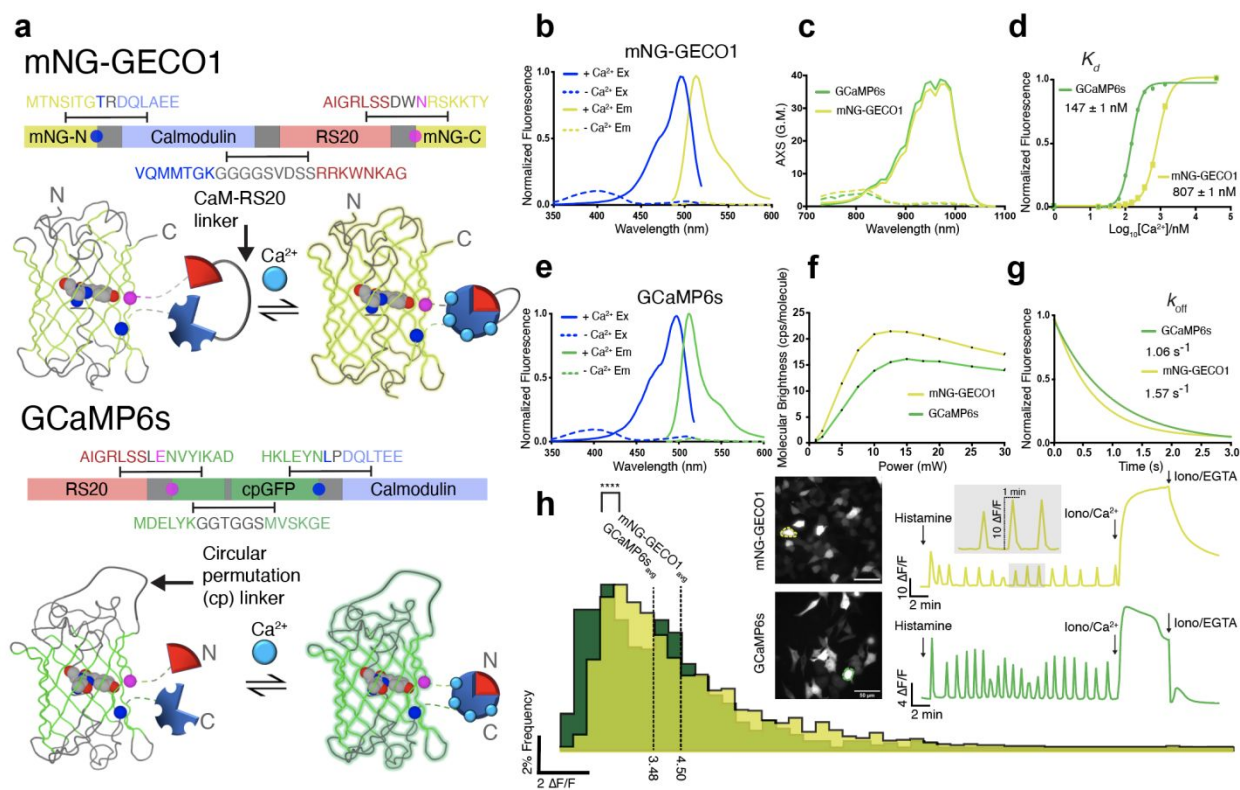


Figure 1 Topology and *in vitro* characterization of mNG-GECO1 and GCaMP6s

a Topology of non-circularly permuted mNG-GECO1 and circularly permuted GCaMP6s. Linker regions are shown in grey and the two residues that flank the insertion site (residue 136 of mNG in blue and residue 139 in magenta; numbering as in PDB ID 5LTR)²³ are shown as circles on both the protein structure and gene schematics. The Ca²⁺ responsive domains are shaded light blue for CaM and light red for RS20. **b,e** Excitation and emission spectra for each indicator. **c** 2-photon cross section for each indicator in Ca²⁺ saturated or Ca²⁺ free states. **d** Ca²⁺ titration for GCaMP6s ($K_d = 147 \pm 1$ nM) and mNG-GECO1 (807 ± 1 nM). **f** Dependence of two-photon molecular brightness on excitation power intervals. **g** Stop-flow kinetics for each indicator showing mNG-GECO1 ($k_{off} = 1.57$ s⁻¹)

1
2
3 and GCaMP6s ($k_{\text{off}} = 1.06 \text{ s}^{-1}$). **h** Characterization of histamine induced Ca^{2+} oscillations
4
5 in HeLa cells with representative traces inset.
6
7
8
9
10
11
12
13
14
15
16
17
18
19
20
21
22
23
24
25
26
27
28
29
30
31
32
33
34
35
36
37
38
39
40
41
42
43
44
45
46
47
48
49
50
51
52
53
54
55
56
57
58
59
60

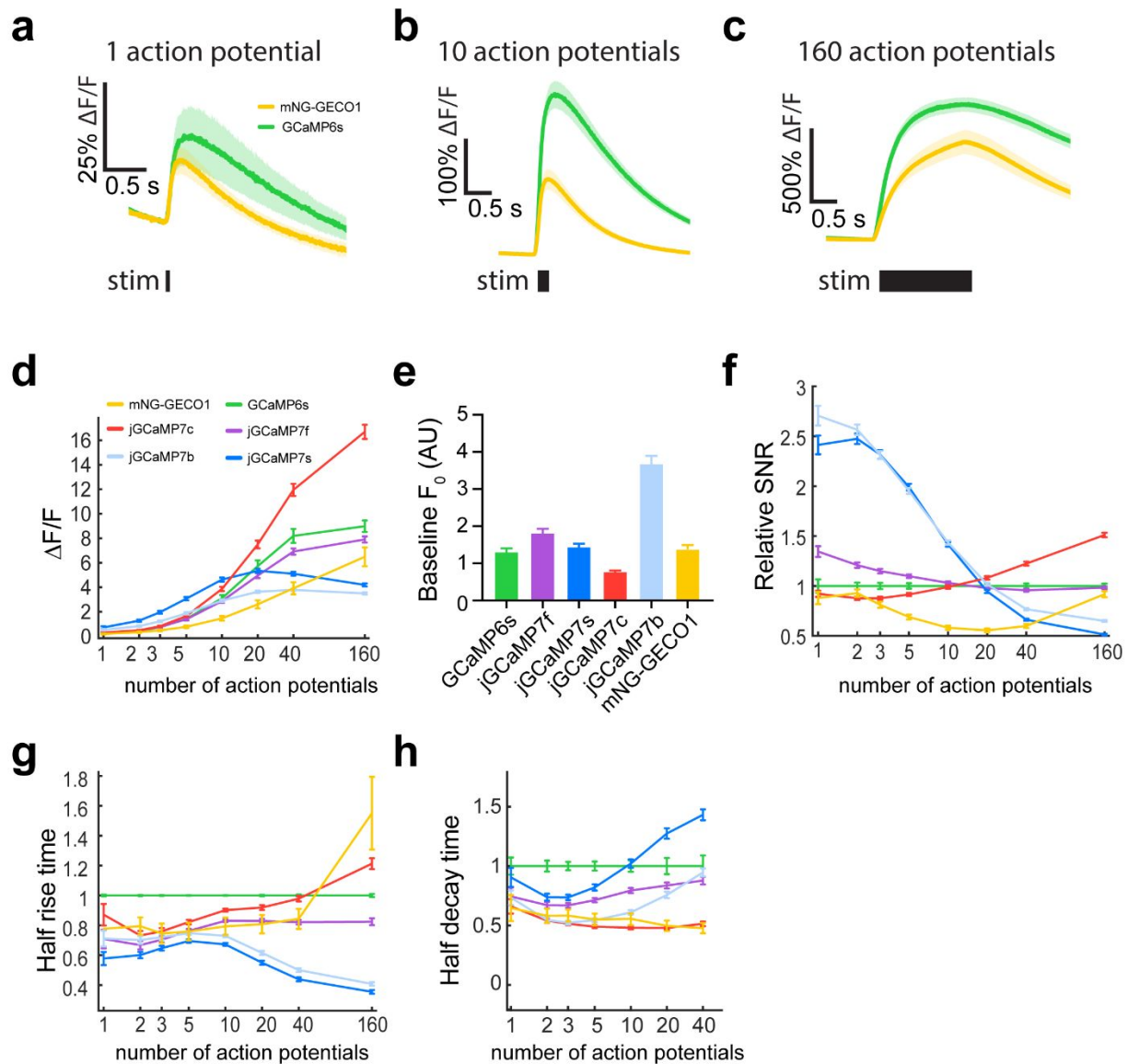


Figure 2 Characterization of mNG-GECO1 and GCaMP series indicators in dissociated rat hippocampal neurons

a-c Average responses to 1, 10, and 160 action potentials for mNG-GECO1 and GCaMP6s. Shaded areas correspond to s.e.m. for each trace. **d** Response amplitude $\Delta F/F_0$ for mNG-GECO1 and the GCaMP series of indicators in response to 1, 2, 3, 5, 10, 20, 40, and 160 action potentials. Data are presented normalized to $\Delta F/F_0$ of GCaMP6s. **e** Baseline brightness for each indicator, defined as the mean raw fluorescence intensity

1
2
3 of all neurons prior to the stimulus. **f** Relative SNR, defined as the peak raw fluorescence
4 divided by the signal standard deviation prior to the stimulus, normalized to SNR of
5
6
7
8
9
10
11
12
13
14
15
16
17
18
19
20
21
22
23
24
25
26
27
28
29
30
31
32
33
34
35
36
37
38
39
40
41
42
43
44
45
46
47
48
49
50
51
52
53
54
55
56
57
58
59
60
of all neurons prior to the stimulus. **f** Relative SNR, defined as the peak raw fluorescence
divided by the signal standard deviation prior to the stimulus, normalized to SNR of
GCaMP6s. **g** Half-rise time normalized to GCaMP6s. **h** Half-decay time normalized to
GCaMP6s. The 160 action potential measurement was omitted because fluorescence
levels generally did not return to baseline over the imaging period. For **a-h**, mNG-GECO1:
621 neurons, 15 wells; GCaMP6s: 937 neurons, 17 wells; jGCaMP7c: 2,551 neurons, 44
wells; jGCaMP7b: 2,339 neurons, 47 wells; jGCaMP7f: 2,585 neurons, 48 wells; and
jGCaMP7s: 2,249 neurons, 47 wells. Data in **d-h** shown as mean \pm s.e.m., see
Supplementary Table 3 for analyzed data.

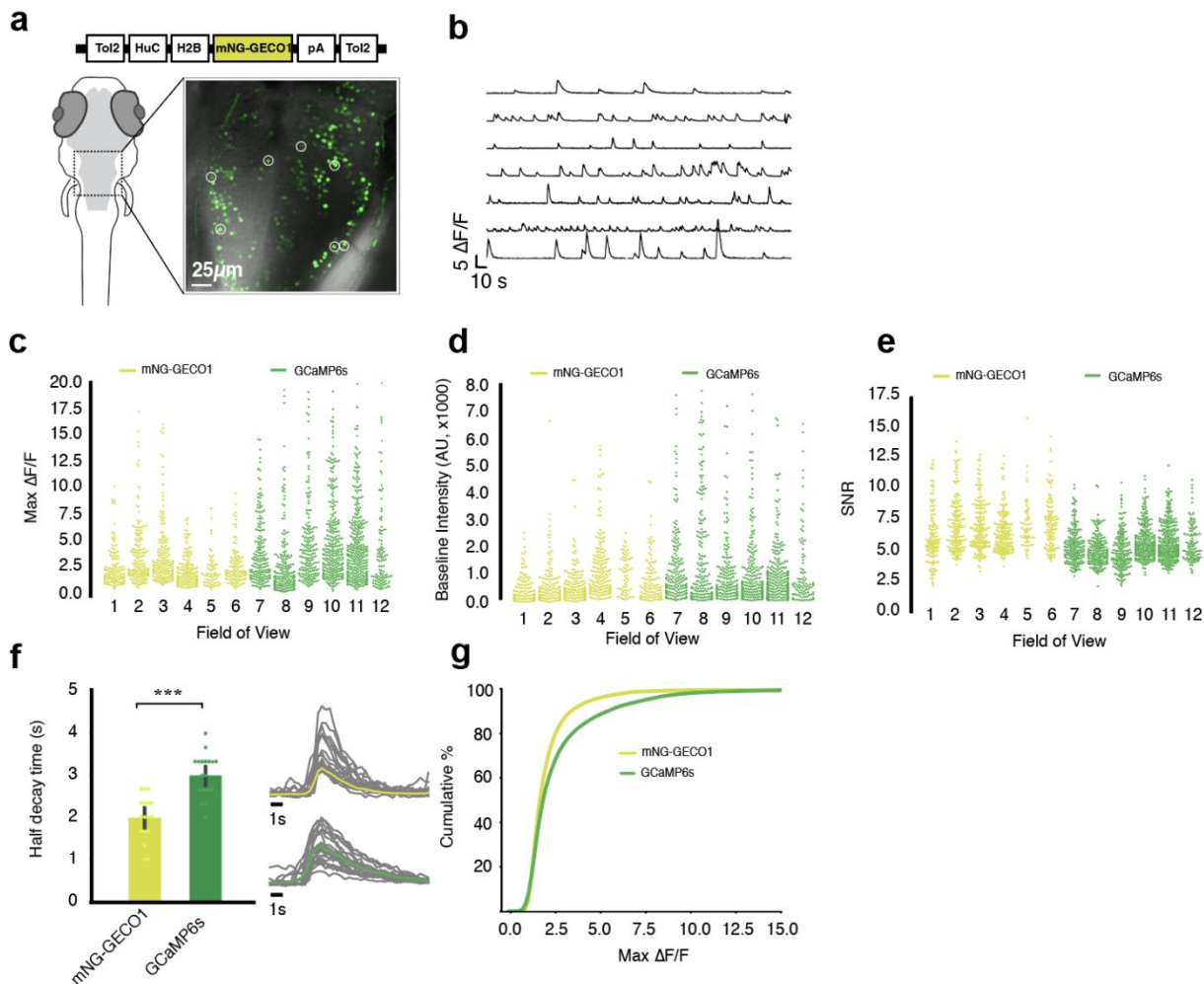


Figure 3 Characterization of mNG-GECO1 and GCaMP6s in transgenic zebrafish hind brain tissue. **a** Schematic representation of Tol2[*HuC-H2B-mNG-GECO1*] construct and confocal image of 1 fish (5 to 6 days post fertilization) with 7 regions of interest (ROI) circled. **b** Traces of ROI's from **a**). **c** Max $\Delta F/F_0$ calculated by taking the max peak of each cell within the field of interest over 5 minutes; 6 ROI's each are used from 5 independent fish expressing mNG-GECO1 and 5 fish expressing GCaMP6s. **d** Baseline fluorescence intensity of each cell within all ROI's from 5 fish; confocal settings are kept consistent between GCaMP6s and mNG-GECO1 imaging. **e** Signal-to-noise ratio (SNR) computed by dividing $\Delta F/F_0$ by raw standard deviation of each cell across 6

1
2
3 FOV's each for both sensors. **f** Average half decay time plotted for mNG-GECO1 (n = 17)
4 and GCaMP6s (n = 19) by averaging randomly selected peaks. **g** Cumulative distribution
5 of mNG-GECO1 vs. GCaMP6s. All cells are arranged in incremental order of $\Delta F/F_0$ and
6 plotted with respect to their $\Delta F/F_0$ and their position in the order (%).
7
8
9
10
11
12
13
14
15
16
17
18
19
20
21
22
23
24
25
26
27
28
29
30
31
32
33
34
35
36
37
38
39
40
41
42
43
44
45
46
47
48
49
50
51
52
53
54
55
56
57
58
59
60

For Table of Contents Only

